The Journal of Nutrition
Aromatic Amino Acids and Related Substances: Chemistry, Biology, Medicine, and Application

3-Dimensional Structures of G Protein-Coupled Receptors and Binding Sites of Agonists and Antagonists[1–4]

William A. Goddard III* and Ravinder Abrol

Materials and Process Simulation Center, Beckman Institute, California Institute of Technology, Pasadena, CA 91125

Abstract

We summarize here recent progress in predicting the 3-dimensional (3D) structure of G protein-coupled receptors (GPCR) and in predicting the binding sites for various agonists and antagonists. These receptors play a critical role in cell communications (dopamine, histamine, epinephrine, and serotonin) and in sensing the outside world (vision, smell, taste, and pain). There are no experimental 3D structures available for human GPCR despite their vital function and importance as therapeutic targets. Indeed, considering every form of life, there is an experimental structure for only 1 GPCR: bovine rhodopsin. Consequently, we developed the MembStruk method to predict the 3D structure without using homology. We then validated our predicted structures by using them to predict their binding sites and binding energies for strongly binding agonists and antagonists. The results were in excellent agreement with available binding and mutation experiments. We will summarize the results for adrenergic receptors, dopamine receptors, chemokine receptors, muscarinic acetylcholine receptors, and a tetrapeptide receptor (mas-related gene C11). J. Nutr. 137: 1528S–1538S, 2007.

G protein-coupled receptors (GPCR)[5] are intrinsic membrane proteins with 7 transmembrane (TM) helices, also called 7TM proteins. They are the largest superfamily in the human genome with >800 GPCR identified, including ~340 nonolfactory receptors organized in 5 families: glutamate, rhodopsin, adhesion, frizzled, and secretin (1). A variety of bioactive molecules (including biogenic amines, peptides, lipids, nucleotides, and proteins) modulate GPCR activity to affect regulation of essential physiological processes (e.g. neurotransmission, cellular metabolism, secretion, cell growth, immune defense, and differentiation). Thus, many important cell recognition and communication processes involve GPCR (2,3). Due to their mediation of numerous critical physiological functions, GPCR are involved in all major disease areas, including cardiovascular, metabolic, neurodegenerative, psychiatric, cancer, and infectious diseases (4,5). Indeed, GPCR represent 30–50% of the current drug targets for activation (by agonist drugs) or inhibition (by antagonists) (5,6). It is estimated that the ~80 GPCR-targeting drugs currently marketed account for ~$50 billion in annual sales, and many have annual sales >$2 billion. Target evaluation, lead identification, and optimization of GPCR have accelerated progress in identifying subtypes with specific cell and tissue functions. However, progress in developing new drugs with reduced toxicity and side effects has been hampered by the lack of a 3-dimensional (3D) structure for any human GPCR or the common animal surrogate targets.

Despite intensive efforts for decades by many protein crystallography groups, the only experimental 3D structure for any GPCR of any form of life is bovine rhodopsin (7). This is due to poor expression levels, difficulties in large-scale receptor purification, the insolubility in media lacking phospholipids, and the difficulty in crystallization. Unfortunately, the homology of bovine rhodopsin with most drug targets is too low (<20%) for use in homology methods to predict structures.

To provide the 3D structures needed to understand the function of GPCR and to help design new ligands, we developed the MembStruk method (8) to predict the 3D structure (without using homology to known 3D structures), which we have applied to predict the 3D structures for ~10 GPCR families. We will summarize here the results for β2 adrenergic receptor (AR), D2

[1] Published in a supplement to *The Journal of Nutrition*. Presented at the "Conference on Aromatic Amino Acids and Related Substances: Chemistry, Biology, Medicine, and Application" held July 20–21, 2006 in Vancouver, Canada. The conference was sponsored by Ajinomoto Company, Inc. The organizing committee for the symposium and Guest Editors for the supplement were: Katsuji Takai, Dennis M. Bier, Luc Cynober, Sidney M. Morris, Jr., and Yoshiharu Shimomura. Guest Editor disclosure: Expenses to travel to the meeting were paid by Ajinomoto Company, Inc. for K. Takai, D. M. Bier, L. Cynober, S. M. Morris, Jr., and Y. Shimomura; D. M. Bier has consulted for Ajinomoto Company, Inc. on scientific issues.

[2] Supported in part by NIH (R21-MH073910-01-A1) and by the Materials and Process Simulation Center. The original funding for this work was through an ARO-MURI (Dr. R. Campbell) and then by Aventis (now Sanofi-Aventis) and Berlex (now part of Bayer-Schering).

[3] Author disclosures: Travel expenses for W. A. Goddard III to attend meeting paid by The Ajinomoto Company, Inc.; R. Abrol, no conflicts of interest.

[4] Color versions of Figures 1, 2, 3, 6, 7, 9, 12, 16, and 17 are available with the online posting of this paper at jn.nutrition.org.

[5] Abbreviations used: AR, adrenergic receptor; Asn, asparagine; Asp, aspartic acid; 3D, 3-dimensional; DR, dopamine receptor; EC, extracellular; EPI, epinephrine; GPCR, G protein-coupled receptor; His, histidine; IC, intracellular; Ile, isoleucine; MAR, muscarinic acetylcholine receptor; MD, molecular dynamics; Mrg, mas-related gene; Phe, phenylalanine; QNB, quinuclidinyl benzilate; Ser, serine; TM, transmembrane; Trp, tryptophan; Tyr, tyrosine; Val, valine.

* To whom correspondence should be addressed. E-mail: wag@wag.caltech.edu.

dopamine receptor (DR), CCR1 chemokine receptor, M1 muscarinic acetylcholine receptor (MAR), and the Mas-related gene (Mrg)C11 receptor. These GPCR families have been the focus of many experimental studies, providing a great deal of binding and mutation experimental data for the validation of our predictions.

After predicting the best structure for each GPCR, we validated this structure by using the HierDock procedure (9) or MSCDock (10) to predict the binding site, binding configuration, and binding energy of known strongly binding ligands. Then we used the predicted structure for the ligand-GPCR complex to predict which mutations would dramatically decrease or increase binding. We have applied HierDock/MSCDock to successfully predict the binding site structure and binding energy of 5–15 ligands to human D2 DR (11), human β2 AR (12), human M1 MAR (13), human CCR1 chemokine receptor (14), and mouse MrgC11 receptors (J. Heo, S.-K. Han, N. Vaidehi, J. Wendel, P. Kekenes-Huskey, and W. A. Goddard III, unpublished results). These predictions have compared well to available experimental binding and mutation data even for larger ligands such as haloperidol and domperidone. Indeed, in some cases, the predictions preceded the experiments.

Our approach was to predict the structures for GPCR without using any experimental data (no constraints). We did, of course, compare our predictions to any available experimental data; however, we did not modify our predicted structures to fit experimental data. Rather, we used any apparent disagreements with experiments to warn us to reexamine our methods and assumptions. This was useful for improving our methods, which now generally give the correct answer for all known cases.

These atomic level 3-D structures are providing a detailed understanding of the structural conformational space of these receptors and their ligand-binding properties, which should allow these structures to be related to functional activities of these important receptors. Given the importance of GPCR physiologically and as pharmacologic targets, the results may provide useful new insights of broad biological and medical importance.

Results

This section presents and analyzes the predicted structures for several GPCR systems, all of which were validated by comparison to experimental data. These predictions (using the MembStruk and HierDock/MSCDock methods) encompass a broad range of GPCR systems: adrenergic, dopamine, muscarinic acetylcholine, chemokine, and peptide (MrgC11) receptors. We found excellent agreement with available experimental data for several agonists and antagonists of each system. Although these predictions were first principles in the sense that no experimental atomistic structures or binding data were used in the predictions, it is legitimate to wonder whether such good results could be achieved (predicted) for systems in which the answers were not known. Thus, we include here results for 2 systems (CCR1 and MrgC11 receptors) on which the critical mutation experiments were carried out after all predictions had been completed.

Structure and function of β2-AR

The first extensive validation of the MembStruk and HierDock methods was for the 3D structure of agonists and antagonists bound to β2 AR (12). **Figure 1** shows the overall structure, whereas **Figure 2***A* shows the details of the predicted structure for epinephrine (EPI) bound to human β2 AR. We predicted that: *1*) the amine group of EPI makes a 2.9-Å salt bridge with aspartic acid (Asp)-113 (TM3); 2) the 2 catechol hydroxy groups

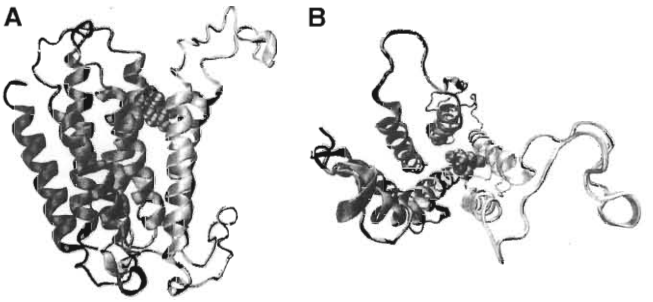

FIGURE 1 Predicted 3D structure of β2 AR with bound EPI. (*A*) Side view. (*B*) Top view.

make hydrogen bonds to the 3 serine (Ser) in TM5 [the 4 hydrogen bond distances are 2.94 Å (Ser-204-meta OH), 3.05 Å (Ser-207-para OH), 3.14 Å (Ser-203-meta OH), and 3.00 Å (Ser-203-para OH)]; 3) asparagine (Asn)-293 make a hydrogen bond to the alkyl OH of EPI; and *4*) phenylalanine (Phe)-290 makes a hydrophobic contact with the aromatic ring of EPI.

An extensive series of mutation and binding experiments was carried out in the late 1980s and early 1990s at Merck [reviewed in (15)] to deduce the residues of β2 AR in contact with EPI (Fig. 2*B*). All 4 elements of the predicted binding site showed essentially exact agreement. In particular, the experiments showed that Ser-204 interacts specifically with the meta hydroxyl, whereas Ser-207 interacts specifically with the para hydroxyl (15), as in the predicted binding site. The experiments showed Asn-293 to be important to binding but did not indicate whether

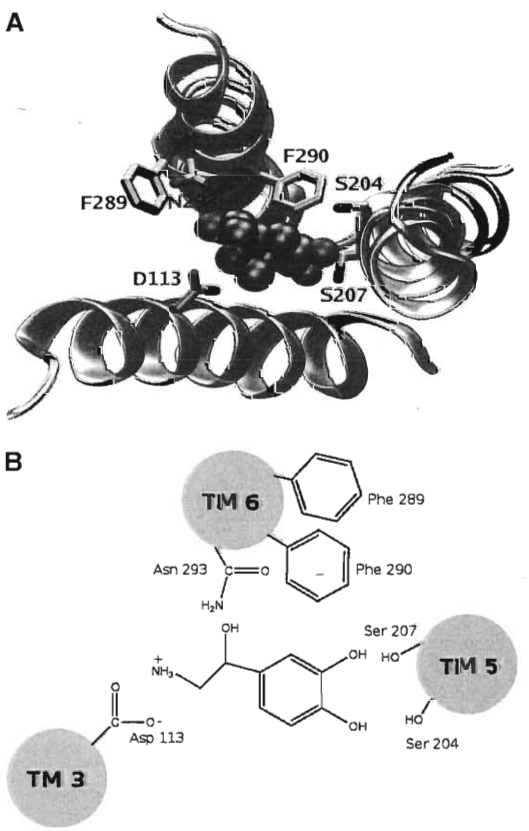

FIGURE 2 (*A*) Critical residues in the predicted binding site for EPI bound to β2 AR. (*B*) Critical residues for EPI bound to β2 AR deduced from multiple experimental mutation and binding studies (15).

it interacted with the amine or alkyl OH part of EPI. Our results indicated that it is the alkyl OH. The experiments indicated some lesser role of Phe-289; we found that it played a stacking interaction with Phe-290. Our results also indicated that Ser-203 interacts with both the meta and para OH groups to form the elegant hydrogen bonding network (**Fig. 3**). The original experiments found no role for Ser-203 in agonist binding, but later experiments found Ser-203 to interact with the meta OH of EPI (16). Binding of phenylephrine (EPI without the para OH) was not substantially affected by mutation of Ser-203 (16). Other residues we predict to be involved in EPI binding are tryptophan (Trp)-109 and valine (Val)-117 in TM3, isoleucine (Ile)-169 in TM4, and alanine-200 in TM5. Thus, EPI binds in a somewhat hydrophobic cavity near the top of TM helices 3–6. We then used HierDock to predict the binding sites and binding energies for 10 agonists and antagonists. We found that the binding sites of these 10 ligands showed consistent patterns in the binding site. Thus, the agonists EPI, norepinephrine, salbutamol, and isoproterenol all formed hydrogen bonds with both Ser-204 and Ser-207, the antagonists that bind strongly to the receptor form hydrogen bonds only with Ser-203 (or Ser-203 and Ser-204 for butoxamine), but never Ser-207. Both agonists and antagonists had a strong bond to the Asp-113 of TM3.

These results suggest that an agonist must couple strongly to TM5 with both Ser-204 and Ser-207 while also bonding to TM3 through Asp-113. We also found that the antagonists recognized the same site (to block the agonist) but led to a more flexible coupling of TM3 and TM5 while blocking motion between TM3 and TM6.

Dynamic behavior of fully solvated β2-AR, embedded in the membrane with bound agonist or antagonist

To optimize all possible positions of the ligand and all possible packings of the helices while simultaneously describing the structures of the lipid, water, and ions was impractical. To find the correct structures, it was essential that MembStruk and HierDock sample all reasonable configurations of the ligand and protein and, hence, we severely restricted the description of the lipid and solvent so important to the stability of the GPCR-ligand complex. Thus, the calculations used implicit solvent and only ~50 lipid molecules (~2 layers around the TM domain). Then, after predicting the ligand-GPCR complex, we removed these restrictions by embedding the optimum protein-ligand complex in an infinite (periodic) lipid bilayer, embedding the membrane-protein-ligand complex in an infinite (periodic) box of equilibrated water, and adding the appropriate counter ions or salt. We then minimized the full structure (40,000–100,000 atoms), heated gradually to 300 K, and equilibrated the structure for ~10 ns at 300 K.

For the 6 HierDock-MembStruk structures we have tested in this way (several ligands with β2 AR (17), 1 ligand with CCR1 chemokine receptor (14), 2 ligands with M1 MAR (13), we found that the predicted structures remained stable with modest changes in structures and interactions. However, in several systems, a couple of water molecules invaded the active site, often helping to stabilize hydrogen bond interactions. We illustrated this observation with 1 case, β2 AR (17).

Spijker et al. (17) considered 3 systems: human apo-β2 AR, the endogenous agonist EPI bound to β2 AR, and the β2 AR selective antagonist butoxamine bound to β2 AR. A visual indication of the stability of the structure is shown in **Figure 4**, which compares the original structure from the MembStruk-HierDock predictions of EPI-β2 AR (left half of Fig. 4) to the structure after 4 ns of molecular dynamics (MD) simulation in the presence of a full membrane and water (~100,000 atoms). Slight changes occurred in the conformation of the protein (~7° change in tilt for 2 helices, bringing them closer). The EPI moved by ~1.2 Å (accommodating a water near the catechol OH and TM5 Ser), but it retained all of the previous strong interactions with the crucial residues. The biggest changes occurred in the intracellular (IC) and extracellular (EC) loops. These underwent large deformations (as shown in Fig. 4), with C_α-atom root mean squared differences from 3–5 Å.

The dynamics showed considerable differences among the 3 cases studied. Thus, the antagonist-β2 AR complex was very rigid with little motion between TM3 and TM6 or elsewhere. In apo-β2 AR, the conserved Ser of TM5 interacted with TM4 rather than pointing to where the catechol OH of the agonist would bind. However, in the dynamics, it was clear that TM5 was quite flexible with significant oscillatory motions toward the region where the agonist would bind. Overall, the apo-β2 AR was much more dynamic than the antagonist-β2 AR complex. In contrast, the EPI-β2 AR complex showed large dynamic fluctuations, much more than apo-β2 AR and far more than the antagonist-β2 AR complex. The dynamics of the EPI-β2 AR

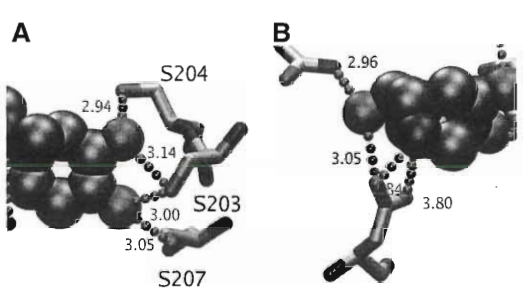

FIGURE 3 Important contacts in the predicted binding site of EPI to human β2 AR. (*A*) The hydrogen bond network formed between both catechol OH groups with S203, S204, and S205 of TM5. (*B*) The hydrogen bond network formed between D113 and N293 with the amine and hydroxyl (12).

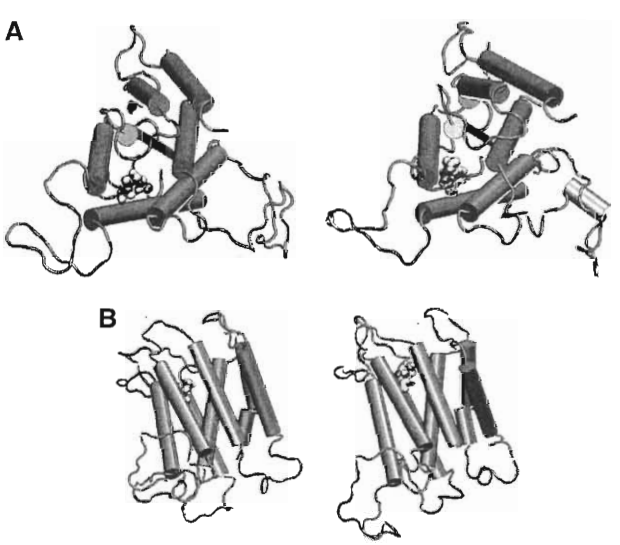

FIGURE 4 The structure of EPI-β2 AR at the start (left) and after 4 ns of MD simulations (right). (*A*) Orthogonal top view. (*B*) Side view. The figure shows that the largest changes are tilts in helices 3 and 4 by an additional 6° and 7° with respect to the surface normal of the lipid bilayer. The protein is shown in a cartoon, and the EPI is shown as van der Waals spheres (17).

complex showed considerable fluctuations in the TM3–TM6 regions and one can imagine it is ready to do something dramatic (of course, to simulate an actual activation event would likely take far longer than 10 ns).

Figure 5 shows the variation over 6 ns of various nonbond distances of EPI (upper) or butoxamine (lower) to the residues of β2 AR. They showed that the salt bridge between the Asp-113 (TM3) and the protonated amine was preserved throughout the dynamics for both ligands (arrows 1 and 2), leading to an average length of 2.8 Å for EPI-β2 AR and 3.0 Å for butoxamine-β2 AR. The ligand-protein hydrogen bonds, however, fluctuated during the dynamics. The hydrogen bond between the meta-catechol OH group of EPI with Ser-203 (TM5) was maintained as a direct hydrogen bond for ~0.8 ns (breaking at arrow 3) and as a water-mediated hydrogen bond for another 0.8 ns (breaking at arrow 4). The hydrogen bond between Asn-293 and the alkyl OH group of EPI was lost near the beginning of the simulation (arrow 3) but formed again after 2 ns (arrow 5). Most hydrogen bonds between TM4 (Ser-165) and TM5 (Ser-204) were lost almost immediately (arrow 3). During the MD simulations, butoxamine continued to exhibit hydrophobic interactions with histidine (His)-172 (TM4), Trp-286 (TM5), and Ile-294 (TM6). Figure 5 shows that these interactions remained tight through the entire MD run. We found that the hydrophobic interactions with Val-119, Ile-169, and Phe-290 remained rather constant (~4.5 Å) throughout the MD run.

In summary, the predicted structures for apo-β2 AR and butoxamine-β2 AR were stable in MD, but in EPI-β2 AR, EC water entered the binding pocket to mediate hydrogen bonding between the catechol of EPI and Ser-204 on helix 5. The EPI-β2 AR structure showed dynamic flexibility with small, piston-like movements of helices 3 and 6 and transient interhelical hydrogen bonding between Ser-165 on TM4 and Ser-207 on TM5. These couplings and motions may play a role in protein activation. The apo-β2 AR showed less dynamic flexibility, whereas the antagonist-β2 AR structure was quite rigid.

This MD validation of the structure predictions for GPCR in explicit lipid and water suggests that these methods lead to predicted 3D structures sufficiently accurate for predicting the binding sites of agonists and antagonists. Thus, it should be possible to use these structures to design subtype-specific ligands.

The changes in the interhelical hydrogen bonding between TM 4 and 5 as the agonist binds were most interesting, remaining fairly stable throughout the simulation. In addition, the incorporation of water-mediated hydrogen bonds showed that water can play a critical role in ligand binding. The differences in the simulations among the antagonist-protein, the agonist-protein, and the apo-protein structures indicated that 6 ns of simulation was already sufficient to show differences between agonist and antagonist. Such differences should be testable experimentally.

Although we found that the agonist-β2 AR dynamics differed substantially from the dynamics of the apo-protein and antagonist-protein of systems, we did not expect such simulations to be sufficiently long to follow the activation events. We are now extending our procedures to generate an ensemble of low-lying structures with agonist bound with the hope that some of these will correspond to intermediates in the process of activation, providing structural information that could be used to design experimental tests.

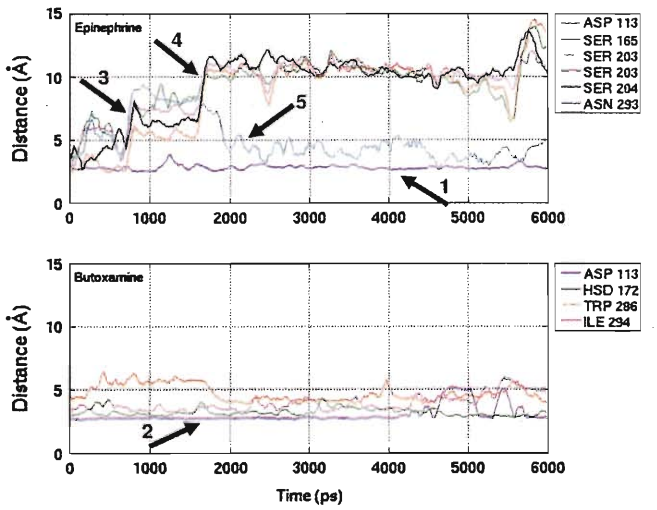

FIGURE 5 Variation of nonbond distances with time for several residues in the β2 AR. (Top) EPI-β2 AR. (Bottom) Butoxamine-β2 AR. The different residues are listed in the legends to the right. For Ser-203, we report the distances to both 2 OH groups of the catechol moiety of EPI. The arrows indicate specific events, which are discussed in the text (17).

Prediction of structure and function for human D2 DR

There are 5 human DR, usually partitioned into 2 subfamilies. DR1 (consisting of the D1 and D5 receptors, which have an 82% sequence identity) and DR2 (consisting of D2–D4, which also have high sequence identity), with a sequence identity between D1 and D2 of only 44%. The DR2 class has a long 3rd IC loop and a short carboxyl terminus, whereas the DR1 class has a short 3rd IC loop and a long carboxyl terminus. Such differences are likely to cause functional differences between these classes of the receptors. Certainly, the differences in the length of the 3rd IC loop could affect the interaction with the G-protein.

Kalani et al. (11) used MembStruk to predict the 3D structure of the human D2 DR from the primary sequence and used HierDock to predict the binding site for dopamine and 10 other ligands. The predicted binding site for dopamine (see **Fig. 6**) and for other agonists is located between TM helices 3–6. The residues in contact with dopamine in the predicted binding site (shown in **Fig. 7**) are in excellent agreement with the results from the mutation studies.

Binding site of dopamine. Kalani et al. (11) predicted that dopamine, the endogenous ligand of the DR, binds in a site

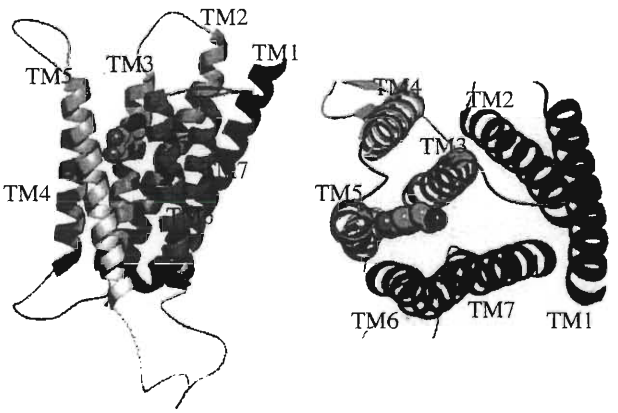

FIGURE 6 Predicted binding site of dopamine (shown in spheres) in the predicted structure of human dopamine D2 receptor (11).

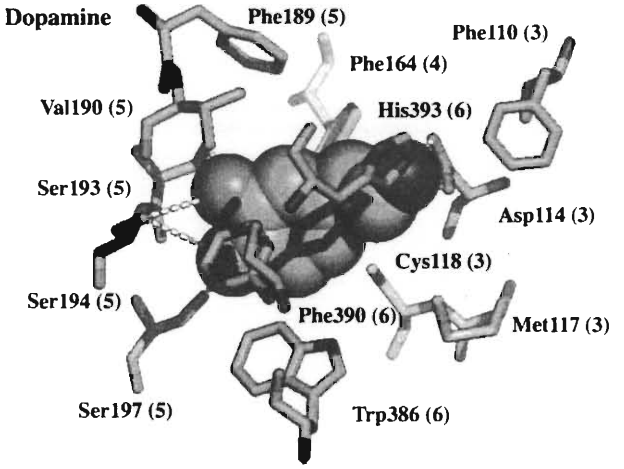

FIGURE 7 Residues within 5.5 Å of the bound dopamine in the human dopamine D2 receptor. The numbers shown in parentheses are the TM helix to which the residue belongs. The distance between Asp-114 and the primary amine group in dopamine is 2.6 Å. Ser-193 on TM5 makes a 2.7-Å hydrogen bond with the metahydroxyl group and Ser-197 makes a 2.7-Å hydrogen bond to the parahydroxyl group of dopamine (11).

located between TM 3–6 (see Fig. 7). They found 2 main contacts that stabilize dopamine in this docked conformation: *1*) a salt bridge between the TM3 Asp-114 (bidentate, 2.6 Å and 2.8 Å). This residue has been implicated in direct ligand binding by mutation studies [reviewed in (18)]; and *2*) a network of hydrogen bonds to the TM5 Ser-193, Ser-194, and Ser-197. In our structure, Ser-193 and Ser-197 both had 2.7-Å interactions with the catechol hydroxyls. These residues have been implicated in ligand recognition by mutagenesis studies (15,19).

Other residues in the binding pocket provided a mostly hydrophobic packing for the ligand. These residues included TM3 (Phe-110, methionine-117, and cysteine-118), TM4 (Phe-164), TM5 (Phe-189 and Val-190), and TM6 (Trp-386, Phe-390, and Trp-393). Although Trp-386 and Phe-390 of the well-conserved WXXFF motif on TM6 were within 5 Å of the dopamine-binding site, Phe-389 was slightly (>5.5 Å) away from dopamine (20,21). Kalani et al. (11) found that His-393 in TM6 provided a very strong component of the binding energy of dopamine to the receptor. Because Asp-114 can form either a bidentate salt bridge or a salt bridge and a hydrogen bond to the amino group of dopamine, the interaction with His-393 fulfills the ability of the amino group to form favorable interactions with any other residues.

Agonists- vs. antagonists-binding site. To validate further the predicted structure for D2, Kalani et al. (11) used HierDock to predict the binding configuration and the relative binding affinities of 3 known dopamine agonists (antiparkinsonian) and 7 known antagonists (antipsychotic) in the D2 receptor (**Fig. 8**). For each of these ligands, the entire molecular surface of D2 receptor was scanned using the ScanBindSite procedure (9). For these agonists, the predicted binding site is located between TM–6. From the binding mode of agonists, it was speculated that the agonist binding pulls TM3 and TM5 closer together while allowing flexibility for the motion of TM6.

The 7 antagonists studied here were classified into 2 classes of antagonists. Class I antagonists are bulky (like the tricyclic ring in clozapine) and bind to the same region between TM3–6, similar to the agonist.

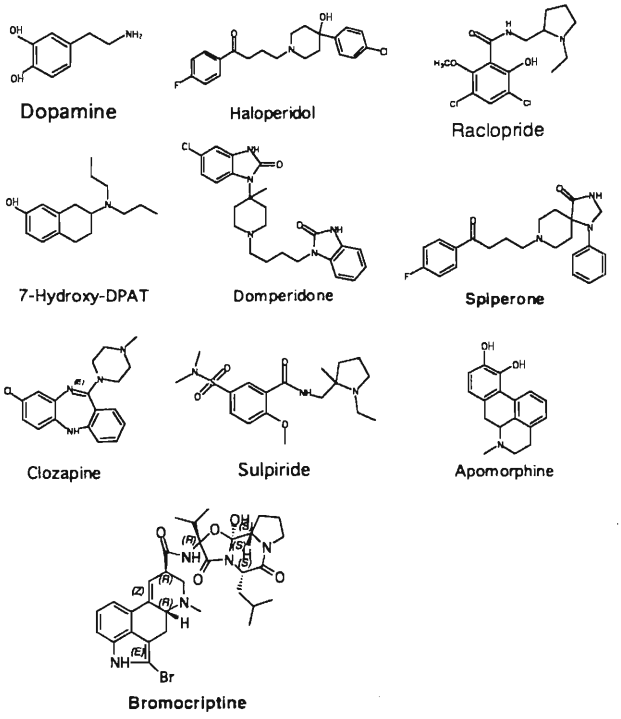

FIGURE 8 Ten agonists and antagonists studied for the human dopamine D2 receptor (11).

Class II antagonists are long molecules with aromatic moieties at each end connected by a flexible linker containing a protonated amine (e.g. haloperidol). Thus, one aromatic moiety occupies the hydrophobic pocket formed by TM3–6, whereas the other occupies the hydrophobic pocket formed by TM2, 3, and 7. The relative location of the agonist- vs. antagonist-binding sites is shown in **Figure 9**. The residues within 5.5 Å of the clozapine-binding site are shown in **Figure 10***A* and that of class II antagonist haloperidol are shown in Figure 10*B*. Also listed are the residues implicated by mutation experiments to be involved in binding of agonists and antagonists. Such residues found within 5 Å of the predicted structure are colored black in the list in Figure 10*B*. The residues in red are residues that experiment (18) found to affect binding affinity of the antagonist but were not found by theory. The residues listed in blue are predicted within 5 Å of the binding site but have not yet been studied experimentally. Thus, the predicted binding site agrees well with the mutation experiments (18,22–25).

Kalani et al. (11) found characteristic differences between the binding sites of agonists and antagonists. All 7 antagonists studied here make a tight contact to Asp-114 in TM3, but none forms strong contacts to both Ser residues in TM5. In contrast, we observe that all agonists have strong coupling to Asp in TM3

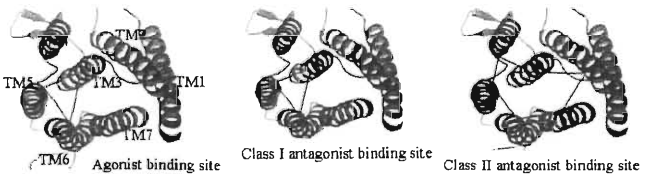

FIGURE 9 Location of the predicted binding sites of dopamine agonists and antagonists in the D2 DR.

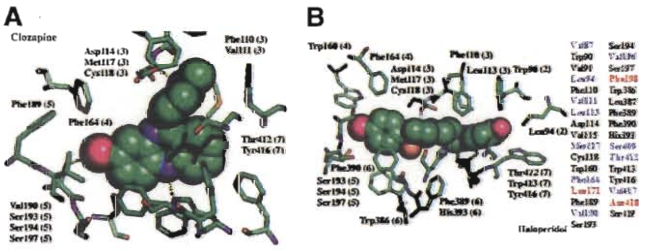

FIGURE 10 (*A*) Residues of the human dopamine D2 receptor within 5.5 Å of the bulky class I antagonist, clozapine. (*B*) Residues within 5.5 Å of the class II antagonist haloperidol. The list of residues shown on the right is the residues that affect ligand binding. The residues colored black in the list are found both by theory and experiments to be important in ligand binding. The residues in blue are predicted by theory but have not been tested experimentally. The residues in red are tested experimentally and are not within 5.5 Å of the predicted binding site (11).

and both Ser in TM5. This suggests that strong coupling between TM3 and TM5 is essential for dopaminergic transduction. This is consistent with experiments (19) showing that hydrogen bonds to both conserved Ser of TM5 are essential for dopamine activation.

Comparison of antagonist-binding sites.

Class I antagonists. The clozapine-like antagonists form a salt bridge to the TM3 Asp-114 with their protonated amino group. They have just 1 aromatic moiety and therefore utilize the aromatic microdomain between TM4 and TM6 (24). They form only 1 weak interaction with the TM6 Ser network, as also for both class I and class II antagonists. The Kalani results indicate that the interaction may be with Ser-193 or Ser-197. These calculations suggest that both the number and strength of the interactions with the TM5 Ser are important for activation. However, the situation must be more complicated, because Strange et al. (26) identified a nonhydroxylated member of the DPAT series as a weak agonist.

The critical distinguishing feature of an agonist vs. an antagonist appears to be its relative position to TM6. Class I antagonists bury their aliphatic domain deep into the conserved TM6 WXXFF motif. Experimental studies on rhodopsin suggest that motion of TM3 and TM6 is necessary for activation (27). The binding of antagonists at the TM6 WXXFF would prevent such motion, specifically the hinge motion between TM3 and TM6 that is likely necessary for activation. The class I antagonists are further stabilized by Phe-110 in TM3.

Class II antagonists. The protonated amino group of haloperidol-like antagonists forms a salt bridge to TM3 Asp-114. This leaves aromatic ring moieties at both ends. In most cases, only 1 of the aromatic rings is halogenated and this ring binds to the first TM46 aromatic microdomain, with the second ring binding in the TM27 aromatic microdomain. The halogenated ring binds effectively into the cavity between TM4 and 6 to form weak interactions with either Ser-193 or Ser-197 in TM5. It gains stability from the presence of TM4 Trp-160 and Phe-164 and TM6 Trp-386 and Phe-390. In some cases, His-393 (TM6) may also stabilize the class II antagonists. The nonhalogenated aromatic domain located in the cavity between TM2 and TM7 gains stabilization from Trp-90 (TM2), Phe-110 (TM3), Trp-413 (TM7), and tyrosine (Tyr)-416 (TM7). As for class I, the class II antagonists prevent motion between TM3 and TM6 by burying their aliphatic portion between TM3 and TM6, thereby preventing interaction of these helices. There is little difference between the binding sites of the class II antagonists, although some more fully utilize the cavity.

Figure 11 compares the calculated binding energies with experimental $\ln K_d$ values. It is difficult to validate the accuracy of the predictions, because the experimental K_d values for a given ligand and receptor often vary by factors of 10 or 20. Generally, the trend of calculated binding energies agrees with the trend of experimental K_d values and usually ligands with binding constants that differ by a factor of 10 are properly ordered. It may seem surprising that the theory does so well at predicting the binding site but only marginally at predicted binding energy. There are 2 problems here. One is that the binding energy is the difference between the energy of the ligand-protein complex and that of the separate ligand and protein complexes. We generally do little to optimize these separate species, usually just removing the ligand, minimizing (to remove strain), and solvating. The 2nd problem is that the calculated binding energies are for minimized structures. That is, we ignore dynamical effects, including entropy. We plan to use the full solvent dynamics at 300 K to extract entropy and enthalpy information, but long time scales may be required to obtain significant results.

Predictions of the 3D structure of the CCR1 chemokine receptor and the BX 471 antagonist-binding site, with subsequent experimental validation

The 18 human chemokine GPCR are important drug targets for such autoimmune diseases as multiple sclerosis and for blocking HIV-1 entry. CCR1 responds to a number of ligands, particularly those associated with a wide variety of autoimmune and pro-inflammatory diseases. This made the CCR1 GPCR an attractive therapeutic target. In particular, Berlex developed BX 471, a potent, orally available specific antagonist to CCR1, currently in phase II clinical trials. To resolve some puzzles in the structure-activity relations and to explain significant differences between the effect of BX471 on human and an animal model, we used MembStruk to predict the 3D structure of the human CCR1 receptor and HierDock to predict the binding site of BX 471 (14). These results explained a variety of structure-activity relations data and some puzzles regarding differential binding in animal models.

The predicted structure for BX 471 bound to the predicted structure of the CCR1 receptor is shown in Figure 12. The

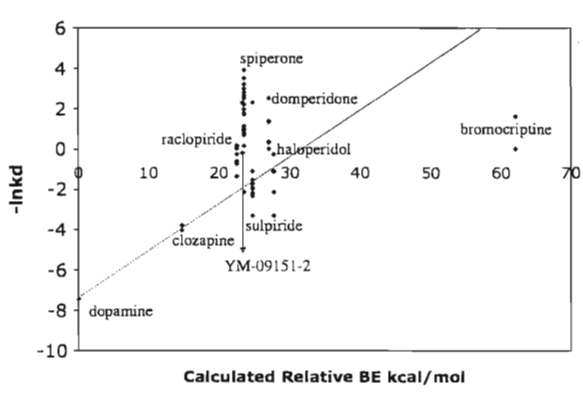

FIGURE 11 Comparison of the calculated binding energies (kilocalories/mole) to the measured binding constants ($-\ln K_d$) for ligands of the human dopamine D2 receptor. The calculated binding energies are at 0 K and have no explicit entropy term included in the calculation (11).

binding site is located between TM3 and TM7. The strongest protein-ligand interactions are of hydrophobic character, arising from Y113 (TM3) and I259 (TM6), which anchor the piperazine ring, and Y114 (TM3), which provides pi-stacking interactions to the adjacent phenyl ring with the urea group. Neither Tyr forms strong hydrogen bonds to BX 471. The fluorine on BX 471 interacts favorably with 1 of the methyl groups of leucine-87 and with the phenyl ring of Phe-83. The urea group of BX 471 does not make tight polar interactions with the protein (one might have expected it to form a hydrogen bond to the carbonyl group of the glycine-168 backbone or the OH-group of Tyr-114). MD simulations of the CCR1/BX 471 complex in explicit lipid bilayer and water indicate that this group is highly flexible and forms hydrogen bonds with water molecules that enter the binding region. The possible contribution of residues in the loop to binding was not included in these calculations.

After predicting the structure of the BX471/CCR1 complex, Vaidehi et al. (14) predicted the effect of 10 mutations on the binding, as shown in the last column of **Table** 1: 3 mutations were expected to reduce binding dramatically, whereas 7 mutations were predicted to have modest effects. Subsequently, Berlex arranged to test these predictions. The CCR1 point mutants were tested for the ability of BX 471 to displace the specific binding of ^{125}I-CCL3 to the wild-type and mutant receptors (Table 1). These competition-binding assays revealed that the mutations Y113A and Y114A on TM3 and I259A on TM6 led to the binding of BX 471 reduced by >500, in line with the data from the chemotaxis assays. Specifically, whereas the antagonist binds to the wild-type receptor with an IC_{50} of 10 nmol, the IC_{50} for the Y113A and I259A mutants is higher than 10 μmol, and for Y114A it is >5 μmol, confirming the predictions. This large decrease in binding energy predicted for Y113A, Y114A, and I259A arises predominantly from the loss of favorable van der Waals interactions of the phenyl-containing residues with the piperazine ring in BX 471. Indeed, the calculations predicted and experiment confirmed that replacement of Y113 by Phe (Y113F) has a minimal effect on the ability of BX 471 to inhibit binding or chemotaxis, compared with a total inability of the antagonist to inhibit either process in the Y113A mutant (Table 1). Note that Y41, Y113, and E287 were previously shown to be important in the binding of the protonated antagonist UCB3562519, whereas E287 and Y113 were implicated in the binding of another protonated antagonist, BX 51018. In contrast, these residues play only a minor role in the calculations with BX 471, a neutral antagonist, where Y113, Y114, and I259 are the most important for ligand binding. Thus, the binding site of the neutral antagonist BX 471 is shifted toward helices 5 and 6 compared with the binding site of protonated antagonists, which lies closer to helices 1 and 2.

TABLE 1 Summary of experiments to test the predicted effects of CCR1 mutations on BX471 inhibition of receptor binding and chemotaxis

Mutant	IC_{50} BX 471 inhibit binding, *nmol*	Ratio	Calculated change in BE
Wild type	10 ± 5	1	0.0
Y113A	>10,000	>1000	6.28
I259A	>10,000	>1000	5.79
Y114A	5017 ± 1970	502	9.24
I91A	849 ± 287	85	−0.55
Y291A	542 ± 308	54	0.04
Y113F	464 ± 164	46	1.49
T86A	348 ± 180	35	−0.52
E287Q	344 ± 122	34	0.06
Y41A	264 ± 179	26	0.02
L260A	58 ± 6	6	0.03

All 3 residues predicted to be critical to binding caused very dramatic decreases in binding, whereas only small effects were observed for the other 7 mutations. Change in binding energies (BE) is calculated as the difference in binding energy of BX 471 in the wild type to the mutant. Binding energy = potential energy of ligand (in protein) – potential energy of ligand (in solvent). Binding energies are reported in kilocalories/mole and do not include room temperature effects or entropic contributions (14). Table reproduced with permission from The American Society for Biochemistry and Molecular Biology.

Finally, Vaidehi et al. (14) used the predicted and validated structure of CCR1 in a virtual screening validation of the Maybridge database seeded with selective CCR1 antagonists. The screen identified all CCR1 antagonists in the top 5% of the hits. These results validate that MembStruk and HierDock lead to structures sufficiently accurate for rational drug design.

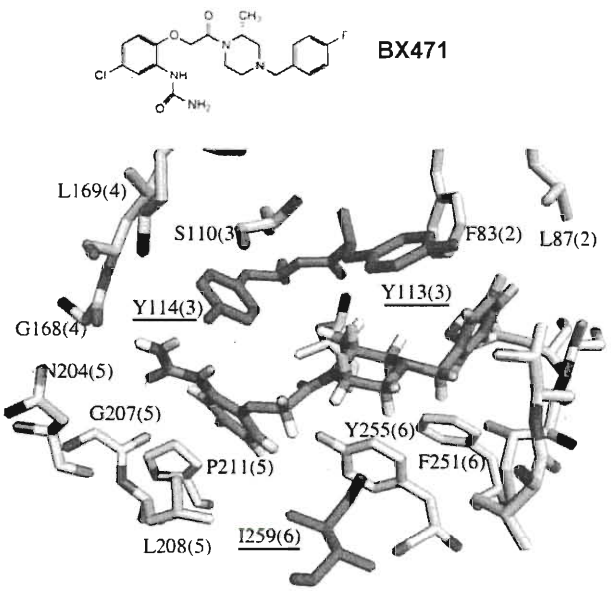

FIGURE 12 Predicted binding site of BX471 antagonist to human CCR1. Details of the predicted binding site (top view) showing all residues within 5 Å for the BX 471 ligand. The underlined residues (Tyr-113, Tyr-114, and Ileu-259) are responsible for anchoring the ligand in this cavity and contribute most to the binding (14). Figure reproduced with permission from The American Society for Biochemistry and Molecular Biology.

Prediction of the 3D structure for FMRF-amide peptides bound to mouse MrgC11 GPCR and experimental validation

Mouse MrgC11 belongs to the Mrg receptor family of GPCR and is localized mainly to isolectin $B4^+$, the small-diameter nociceptors in the dorsal root ganglia likely associated with pain perception. It is not known which endogenous ligand activates mMrgC11 or what function it has, but Dong et al. (28) showed that mMrgC11 is activated by FMRF-amides (Phe-Met-Arg-Phe) and suggested that it is involved in pain sensation or modulation. In particular, Dong et al. (28) showed that mMrgC11 is activated by the F-M-R-F-NH2, (D)F-M-R-F-NH2, and F-(D)M-R-F-NH2 tetrapeptides at ~10–100 nmol concentration, while F-M-(D)R-F-NH2 and F-M-R-(D)F-NH2 are inactive (>10 μmol).

Using MembStruk and HierDock, Heo et al. (J. Heo, S-K Han, N. Vaidehi, J. Wendel, P. Kekenes-Huskey, and W. A.

Goddard III, unpublished results) predicted the 3D structure for mMrgC11 and the binding site for the 5 chiral FMRF-NH_2 ligands, one of which is shown in **Figure 13**. **Table 2** shows that Heo predicted correctly the relative binding observed for the 5 FMRF-NH2 ligands. Thus, Heo predicted that the binding is in the sequence F-(D)M-R-F-NH2 > F-M-R-F-NH2 > (D)F-M-R-F-NH2, as observed experimentally and predicted that F-M-(D)R-F-NH2 and F-M-R-(D)F-NH2 bind far more weakly. The reason for this dramatic dependence on chirality is that first, the RFa (Arg-Phe amide) terminus is buried, interacting strongly with Tyr-110 (TM3), Asp-161 (TM4), and Asp-179 (TM5), then the M comes out of the pocket with little selective binding, and finally, the terminal F sticks back into the pocket, interacting with some Y and W residues. The 2 bad binders have the wrong chirality for the terminal RFa to stick into the primary part of the binding site.

To test the predictions that Y110, D161, and D179 are particularly important, Heo et al. (J. Heo, S-K Han, N. Vaidehi, J. Wendel, P. Kekenes-Huskey, and W. A. Goddard III, unpublished results) constructed experimentally the mutants Y110A, D161A, and D179A, showing that they were expressed equivalently to wild type and carried out IC calcium release assays. These results (Table 2) demonstrate the dramatic decrease in activity for the Y110A, D161A, and D179A mutants predicted by Heo's structures. Thus:

1) The Y110A mutant was not activated by any of the 6 tested ligands, even with concentrations in excess of 33 μmol.
2) For the D161A mutant, 4 of the 6 agonists were rendered inactive, whereas the remaining 2 were active only at 100 times higher concentrations.
3) The D179A mutant showed no affinity for the 3 tetrapeptide agonists, and the other 3 were activated only at 10 times higher concentration of the ligand.

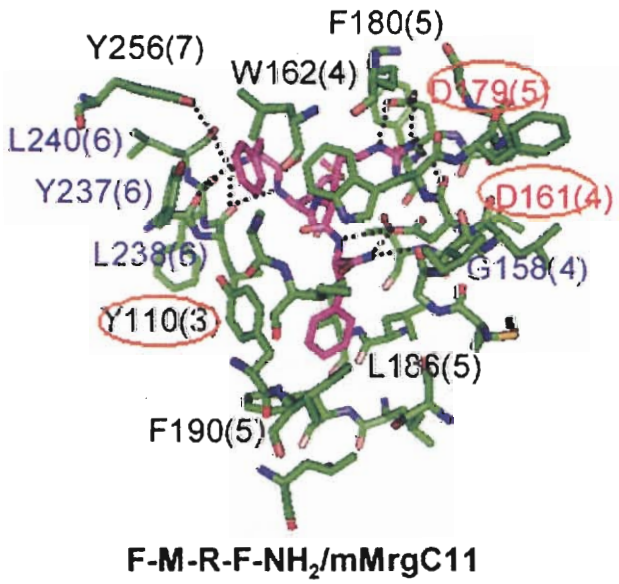

FIGURE 13 Predicted 5 Å binding sites of F-M-R-F-NH_2 to mMrgC11. The intermolecular hydrogen bonds are indicated by the dotted lines. A residue whose side chain participates in the hydrogen bond is specified in red, whereas one whose backbone is involved is in blue. The residues with good hydrophobic interaction are specified in black. The top of the picture corresponds to the EC region (J. Heo, S-K Han, N. Vaidehi, J. Wendel, P. Kekenes-Huskey, and W. A. Goddard III, unpublished results).

These results showing that mutations to alanine of Tyr-110, Asp-161, or Asp-179 eliminate or dramatically reduce binding to mMrgC11 validate both the predicted GPCR structure and the predicted binding site. This validation indicates that it is now practical to predict GPCR structures sufficiently accurately to identify binding sites for selective ligands.

Structure and function of human M1 MAR

All 5 subtypes of MAR have been implicated in the various pathogenetical processes of a wide range of diseases, including cognitive dysfunctions (Alzheimer's disease, Parkinson's disease, and schizophrenia) and smooth muscle disorders (irritable bowel syndrome, overactive bladder, and chronic obstructive pulmonary disease). These receptors have attracted much attention for the design of drug molecules (e.g. agonists for M1 and antagonists for M2) to stimulate the cholinergic system for potential treatment of Alzheimer's disease. The search for M1 receptor agonists has led to a number of drug candidate molecules, many of which had to be discontinued due to undesirable side effects resulting from cross reactivity to other receptor subtypes. Such cross reactivity would likely be greatly reduced by using a structure-based approach for the rational design of drugs coupled with a database of 3D structures to use as antitargets.

Peng et al. (13) predicted the structure of the human MAR 1 (M1) using the MembStruk method and validated this structure by using HierDock to predict the ligand-binding sites for the 7 agonists and antagonists shown in **Figure 14**. The interhelical contacts that stabilize the receptor conformation, the predicted binding sites for agonists and antagonists, and the results of in silico mutagenesis all agree very well with available experimental mutagenesis data. The calculated relative binding energies also reproduce well the order of measured binding affinities.

The predicted binding site of antagonists [quinuclidinyl benzilate (QNB), pirenzepine, *N*-methylscopolamine, and 4-diphenylacetoxy-*N*-methylpiperidine methiodide structures; Fig. 14] is located between TM helices 3–7, whereas the agonist-binding site (tetramethylammonium, acetylcholine, and oxotremorine-M; Fig. 14) involves residues from helices 3, 6, and 7. The overall site is depicted in **Figure 15**, with the QNB antagonist-binding site shown in **Figure 16** and the acetylcholine agonist-binding site shown in **Figure 17**. These antagonist-binding sites provide a structural basis for the large reduction in ligand-binding affinity and signaling efficacy by mutations of Trp-157 (TM4) and proline-159 (TM4). Peng's (13) predictions suggested that Trp-157 (TM4) directly participates in ligand binding instead of forming a secondary ligand docking site, whereas proline-159 (TM4) provides an indirect conformational switch controlling the position of Trp-157 through the kink in Helix 4.

In addition to the critical Asp-105 (TM3), several aromatic residues including Tyr-381 (TM6), Tyr-404 (TM7), and Tyr-408 (TM7) are predicted to be important in binding the ligand quaternary ammonium head group through cation-π interactions (with a geometry similar to that in the nicotinic acetylcholine receptor crystal structure complex). Peng's (13) results also suggest that upon binding of ligands with a charged tertiary amine head group, there might be proton transfer from the ligand to Asp-105 (TM3). In addition, an extensive aromatic network involving Tyr-106 (TM3), Trp-157 (TM4), Phe-197 (TM5), Trp-378 (TM6), and Tyr-381 (TM6) is important in stabilizing the antagonist binding sites (Fig. 16 for QNB antagonist). For antagonists with 2 terminal aromatic rings, this aromatic network extends to Trp-164 (TM4), Tyr-179 (EC loop 2), and possibly Phe-391 (TM6). Asn-382 (TM6) forms hydrogen bonds with

TABLE 2 Binding constants (EC_{50} values in nanomoles) of wild-type and mutant mMrgC11 receptors from IC calcium assays. The predicted binding energies correlate with the measured binding constants

	Binding,[1] %	Wild type	Y110A	D1 61 A[2]	D179A[2]	Y110F	Y110W[3]
FdMRFa	100	113 ± 18	>33,000	>33,000	>33,000	714 (6.3)	334 (3.0)
FMRFa	93	168 ± 26	>33,000	(18,000)[2]	>33,000	1795 (10.7)	1531 (9.1)
dFMRFa	88	276 ± 56	>33,000	>33,000	>33,000	1500 (5.4)	1513 (5.5)
Bam15		292 ± 19	>33,000	>33,000	(3000)[2]	749 (2.6)	1713 (5.9)
γ1-MSH		398 ± 189	>33,000	>33,000	(3000)[2]	331 (0.8)	302 (0.8)
γ2-MSH		340 ± 66	>33,000	(33,000)[2]	(2000)[2]	340 (1.0)	349 (1.0)
FMdRFa	67	>10,000					
FMRdFa	68	>10,000					

[1] Calculated binding energy relative to FdMRFa (absolute value = 117 kcal/mol).
[2] Activation starts at a given concentration.
[3] Number in parentheses is the ratio with respect to the EC_{50} values of the wild type.

selected antagonists. Tyr-381 (TM6) and Ser-109 (TM3) form hydrogen bonds with the ester moiety of acetylcholine, which binds in the gauche conformation.

The predicted structures show the importance of aromatic residues in the binding site, illustrating the cation-π interactions and aromatic-aromatic interactions critical to ligand binding in M1. This study provides an improved structural understanding of the M1 receptor and its binding sites. In addition, it sets the stage for applying these procedures to predict the structures and function of the 4 other muscarinic receptor subtypes, which should enable the development of subtype-specific agonists and antagonists with reduced side effects.

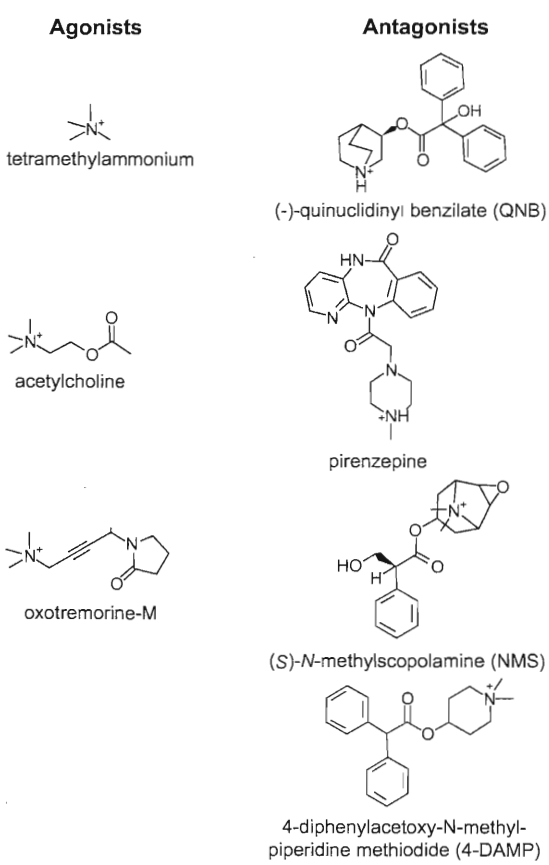

FIGURE 14 Seven ligands used for docking to the M1 acetylcholine receptor (13). Figure reproduced with permission from Wiley VCH.

Discussion

The studies summarized in the preceding section provide a framework for understanding at the atomic level the 3D structures of GPCR and the binding sites for various agonists and antagonists. Such structural information is crucial for the rational design of highly selective therapeutic lead candidates for GPCR targets, leading hopefully to drugs with increased potency and reduced toxicity and other unwanted side effects. Similar studies are in progress in our group for a number of other systems, including the other 8 AR, the other 4 DR, several of the serotonin receptors, 2 other chemokine receptors, the 3 vasopressin receptors, the DP prostaglandin receptor, the Urotensin II receptor, a somatostatin receptor, the 2 cannabinoid receptors, 3 of the 4 histamine receptors, and the other 4 MAR.

Most of the current successes using MembStruk and HierDock have been with the A family of GPCR; however, the methodologies used here should also apply to the other families. Thus, with sufficient funding it would be practical to obtain similar quality structures for all 350 nonsensory receptors of humans over ~5 y. The advantage of having all these structures is that in designing a drug to target 1 of these GPCR, we could use the other 349 as antitargets, minimizing the binding to them. This might provide a means to dramatically reduce cross reactivity, thereby reducing toxic side effects.

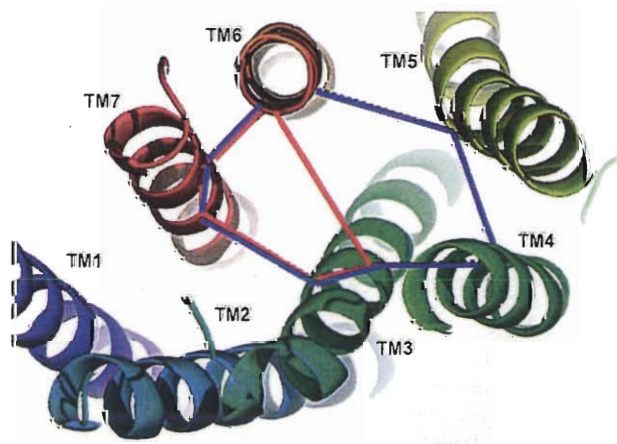

FIGURE 15 Binding regions for antagonists (shown in blue) and agonists (red) in the M1 receptor (13). Figure reproduced with permission from Wiley VCH.

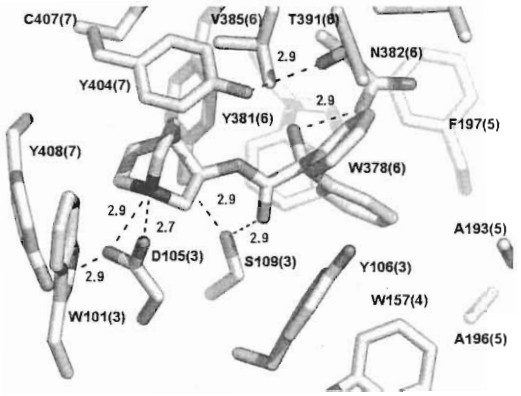

FIGURE 16 The 4-Å binding site of antagonist QNB. The numbers shown in parentheses are the TM helix to which the residue belongs (13). Figure reproduced with permission from Wiley VCH.

We have also reported structures and ligand bonding for ~10 olfactory receptors (9,29–32) and a taste receptor (33). Almost no experimental data on mutations or binding of antagonists exists. In addition, there may be much less selectivity. It would be practical to obtain good quality structures for all ~500 human sensory receptors. A special advantage of doing this might be to compare binding of various odorants and tastes to perceptions by humans of these same odorants and tastes. This might lead to new formulations for perfumes and foods. It might also be useful in training humans or animals to detect odorants associated with diseases or the vapors associated with explosives and nerve gases. Once the structures of ~500 odorant receptors and their binding characteristics for a library of ligands is known, it will be especially interesting to compare the binding strengths (from theory) with the actual perceptions of people along with functional NMR to follow which structures are associated with the perceptions.

It will also be interesting to compare the 3D structures and binding sites of GPCR in mammals with those in other forms of life to better understand the evolution of neural and sensory systems.

Acknowledgments

We have summarized here the major contributions by many members of the Goddard Research Group in the Materials and Process Simulation Center at Caltech. Leading this effort with W.A.G. over the years was Dr. N. Vaidehi (now Professor at City of Hope) and Dr. W. Floriano (now Assistant Professor at Cal Poly Pomona). Major contributions in developing methods were made by Dr. R. Trabanino and Dr. S. Hall and later by J. Wendel, Dr. A. Cho, and in the applications by Dr. Y. Kalani, P. Freddolino, Dr. J. Heo, Dr. P. Spijker, and Dr. J. Peng.

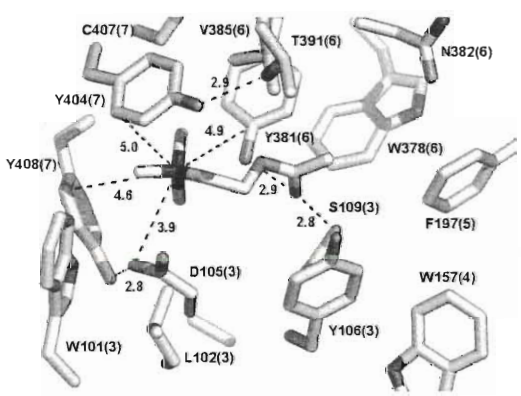

FIGURE 17 The 4-Å binding site of agonist acetylcholine. The numbers shown in parentheses are the TM helix to which the residue belongs. Threonine-391 is not within the acetylcholine-binding distance but is included to illustrate its interhelical hydrogen bond with Tyr-404 (13). Figure reproduced with permission from Wiley VCH.

Literature Cited

1. Fredriksson R, Lagerstrom MC, Lundin LG, Schioth HB. The G-protein-coupled receptors in the human genome form five main families. Phylogenetic analysis, paralogon groups, and fingerprints. Mol Pharmacol. 2003;63:1256–72.
2. Lefkowitz RJ, Pierce KL, Luttrell LM. Dancing with different partners: protein kinase A phosphorylation of seven membrane-spanning receptors regulates their G protein-coupling specificity. Mol Pharmacol. 2002; 62:971–4.
3. Bartfai T, Benovic JL, Bockaert J, Bond RA, Bouvier M, Christopoulos A, Civelli O, Devi LA, George SR, et al. The state of GPCR research in 2004. Nat Rev Drug Discov. 2004;3:575, 577–626.
4. Tang CM, Insel PA. Genetic variation in G-protein-coupled receptors-consequences for G-protein-coupled receptors as drug targets. Expert Opin Ther Targets. 2005;9:12472–65.
5. Lundstrom K. Latest development in drug discovery on G-protein coupled receptors. Curr Protein Pept Sci. 2006;7:465–70.
6. Hopkins AL, Groom CR. The druggable genome. Nat Rev Drug Discov. 2002;1:727–30.
7. Palczewski K, Kumasaka T, Hori T, Behnke CA, Motoshima H, Fox BA, Le Trong I, Teller DC, Okada T, et al. Crystal structure of rhodopsin: a G protein-coupled receptor. Science. 2000;289:739–45.
8. Vaidehi N, Floriano WB, Trabanino R, Hall SE, Freddolino P, Choi EJ, Goddard WA III. Structure and function of GPCR. Proc Natl Acad Sci USA. 2002;99:12622–7.
9. Floriano WB, Vaidehi N, Singer M, Shepherd G, Goddard WA III. Molecular mechanisms underlying differential odor responses of a mouse olfactory receptor. Proc Natl Acad Sci USA. 2000;97:10712–6.
10. Cho A, Wendel JA, Vaidehi N, Kekenes-Huskey PM, Floriano WB, Maiti PK, Goddard WA III. The MPSim-Dock Hierarchical Docking Algorithm: application to the eight trypsin inhibitor co-crystals. J Comput Chem. 2005;26:48–71.
11. Kalani MY, Vaidehi N, Hall SE, Floriano WB, Trabanino RJ, Freddolino PL, Kam V, Goddard WA III. The predicted 3D structure of the human D2 dopamine receptor and the binding site and binding affinities for agonists and antagonists. Proc Natl Acad Sci USA. 2004;101:3815–20.
12. Freddolino PL, Kalani MY, Vaidehi N, Floriano WB, Trabanino RJ, Freddolino PL, Kam V, Goddard WA III. Structure and function prediction for human β2-adrenergic receptor. Proc Natl Acad Sci USA. 2004;101:2736–41.
13. Peng JY, Vaidehi N, Hall SE, Goddard WA III. The predicted 3D structures of the human M1 muscarinic acetylcholine receptor with agonist or antagonist bound. ChemMedChem. 2006;1:878–90.
14. Vaidehi N, Schlyer S, Trabanino RJ, Floriano WB, Abrol R, Sharma S, Kochanny M, Koovakat S, Dunning L, et al. Predictions of CCR1 chemokine receptor structure and BX 471 antagonist binding followed by experimental validation. J Biol Chem. 2006;281:27613–20.
15. Strader CD, Fong TM, Tota MR, Underwood D, Dixon RAF. Structure and function of G-protein coupled receptors. Annu Rev Biochem. 1994; 63:101–32.
16. Liapakis G, Ballesteros JA, Papachristou S, Chan WC, Chen X, Javitch JA. The forgotten serine: a critical role for Ser-203(5.42) in ligand binding to and activation of the beta(2)-adrenergic receptor. J Biol Chem. 2000;275:37779–88.
17. Spijker P, Vaidehi N, Freddolino PL, Hilbers PA, Goddard WA III. Dynamic behavior of fully solvated β2-adrenergic receptor, embedded in the membrane with bound agonist or antagonist. Proc Natl Acad Sci USA. 2006;103:4882–7.
18. Shi L, Javitch JA. The binding site of aminergic G protein-coupled receptors: the transmembrane segments and second extracellular loop. Annu Rev Pharmacol Toxicol. 2002;42:437–67.

19. Teeter MM, Froimowitz M, Stec B, DuRand CJ. Homology modeling of the dopamine D2 receptor and its testing by docking of agonists and tricyclic antagonists. J Med Chem. 1994;37:2874–88.
20. Cho W, Taylor LP, Mansour A, Akil H. Hydrophobic residues of the D2 dopamine receptor are important for binding and signal transduction. J Neurochem. 1995;65:2105–15.
21. Javitch JA, Ballesteros JA, Weinstein H, Chen J. A cluster of aromatic residues in the sixth membrane-spanning segment of the dopamine D2 receptor is accessible in the binding-site crevice. Biochemistry. 1998;37: 998–1006.
22. Fu D, Ballesteros JA, Weinstein H, Chen J, Javitch JA. Residues in the seventh membrane-spanning segment of the dopamine D2 receptor accessible in the binding-site crevice. Biochemistry. 1996;35: 11278–85.
23. Shi L, Simpson MM, Ballesteros JA, Javitch JA. The first transmembrane segment of the dopamine D2 receptor: accessibility in the binding-site crevice and position in the transmembrane bundle. Biochemistry. 2001;40:12339–48.
24. Simpson MM, Ballesteros JA, Chiappa V, Chen J, Suehiro M, Hartman DS, Godel T, Snyder L, Sakmar TP, et al. Dopamine D4/D2 receptor selectivity is determined by a divergent aromatic microdomain contained within the second, third, and seventh membrane-spanning segments. Mol Pharmacol. 1999;56:1116–26.
25. Dijkstra D, Rodenhuis N, Vermeulen ES, Pugsley TA, Wise LD, Wikstrom HV. Further characterization of structural requirements for ligands at the dopamine D2 and D3 receptor: exploring the thiophene moiety. J Med Chem. 2002;45:3022–31.
26. Strange PG. Dopamine receptors: studies on structure and function. Adv Drug Res. 1996;28:313–51.
27. Hubbell WL, Altenbach C, Hubbell CM, Khorana HG. Rhodopsin structure, dynamics, and activation: a perspective from crystallography, site-directed spin labeling, sulfhydryl reactivity and disulfide cross-linking. Adv Protein Chem. 2003;63:243–90.
28. Dong X, Han S, Zylka MJ, Simon MI, Anderson DJ. A diverse family of GPCR expressed in specific subsets of nociceptive sensory neurons. Cell. 2001;106:619–32.
29. Floriano WB, Vaidehi N, Goddard WA III. Making sense of olfaction through predictions of the 3-D structure and function of olfactory receptor. Chem Senses. 2004;29:269–90.
30. Hall SE, Floriano WB, Vaidehi N, Goddard WA III. Predicted 3-D structures for mouse I7 and rat I7 olfactory receptors and comparison of predicted odor recognition profiles with experiment. Chem Senses. 2004;29:595–616.
31. Hummel P, Vaidehi N, Floriano WB, Hall SE, Goddard WA III. Test of the binding threshold hypothesis for olfactory receptors: explanation of the differential binding of ketones to the mouse and human orthologs of olfactory receptor 912–93. Protein Sci. 2005;14:703–10.
32. Trabanino R, Hall SE, Vaidehi N, Floriano WB, Goddard WA III. First principles prediction of the structure and function of G protein-coupled receptors: validation for bovine rhodopsin. Biophys J. 2004;86: 1904–21.
33. Floriano WB, Hall S, Vaidehi N, Kim U, Drayna D, Goddard WA III. Modeling the human PTC bitter-taste receptor interactions with bitter tastants. J Mol Model. 2006;12:931–41.